

Transformation of magnetic phase transition in MnO confined to channel type matrices. Neutron diffraction study.

I. V. Golosovsky

Petersburg Nuclear Physics Institute, 188300, Gatchina, St. Petersburg, Russia.

I. Mirebeau

Laboratoire Léon Brillouin, CE-Saclay, F-91191, Gif-sur-Yvette, France.

V. P. Sakhnenko

Rostov State University, 344090, Rostov/Don, Russia.

D. A. Kurdyukov and Y. A. Kumzerov

A. F. Ioffe Physico-Technical Institute, 194021, St. Petersburg, Russia.

Neutron diffraction studies of antiferromagnetic MnO confined to MCM-41 type matrices with channel diameters $24\div 87$ Å demonstrate that the antiferromagnetic phase transition is a continuous one with an enhanced Néel temperature in contrast to a discontinuous first order transition in the bulk. With decreasing channel diameter, the character of the magnetic transition transforms, showing the reduction of magnetic dimensionality towards a quasi one-dimensional system. Enhancement of the Néel temperature is explained within the framework of Landau theory taking into consideration the interaction of the surface ferromagnetic moment with the antiferromagnetic order parameter.

PACS numbers: 61.12.Ld; 74.78.Na; 75.30.Kz

I. INTRODUCTION

The properties of magnetics confined to nanometer scale cavities drastically differ from those of the bulk that stimulates an interest in the behavior of magnetic materials in the conditions of so-called "restricted" or "confined" geometry. One of the most intriguing problems is the influence of the "confined geometry" on the magnetic phase transition.

We have recently reported that antiferromagnetic MnO embedded in a vycor-glass type matrix with a random network of interconnected pores exposes some remarkable differences when compared to the bulk¹. It was found by neutron diffraction that a first order magnetic transition becomes a second order with the Néel temperature 120.2(1) K slightly higher than 117.6(1) K for the bulk MnO². It was demonstrated that confined MnO forms aggregates with the average diameter of 145(3) Å. Below the magnetic transition a long range magnetic ordering appears within a "core" with a smaller average diameter of about 100(3) Å, and the magnetic moment is reduced.

We continue these studies with MnO confined to the cavities with another topology, namely, to nanochannels of mesoporous MCM-41 type matrices. From synchrotron diffraction experiments we found that MnO confined to the large 47-87 Å channels crystallizes in the form of thin (about 10 Å) ribbon-like structures with a width of about the channel diameter and a length of 180-260 Å. In the matrices with the narrower channels of 24 and 35 Å diameters MnO crystallizes in the form of nanowires with smaller diameters 20 Å and a length of about 180-200 Å³. The morphology of the MnO nanoparticles thus varies

considerably depending on the matrix and can show different dimensionalities of the spin system.

The ESR experiments with the same samples⁴ confirmed the presence and strong influence of the surface disordered spins on the magnetic behavior of confined MnO. However the ordered magnetic moment cannot be studied by the ESR technique and thus other experimental techniques are needed.

In the present study neutron diffraction techniques are used for the same samples to investigate in a more systematic way the effect of nanoparticle size on magnetism in MnO confined to channel-type matrices.

II. EXPERIMENT

A. Experimental details

The experiments were performed with MnO embedded in the channel of MCM-41 matrices⁵ with 24 and 35 Å channel diameters and SBA-15 matrices⁶ with 47, 68 and 87 Å channel diameters, respectfully. These matrices differ by the preparation techniques and both form an amorphous silica (SiO₂) with a regular hexagonal array of parallel cylindrical nanochannels. The matrices in the form of powders with a grain size $\sim 1\text{-}2$ μm were prepared in the Laboratoire de Chimie Physique, Université Paris-Sud, France⁷. All samples were filled with MnO from a solution by the "bath deposition" method developed in the Ioffe Physico-Technical Institute (St Petersburg, Russia). The consistent analysis of neutron diffraction, X-ray diffraction, ESR and magnetization measurements

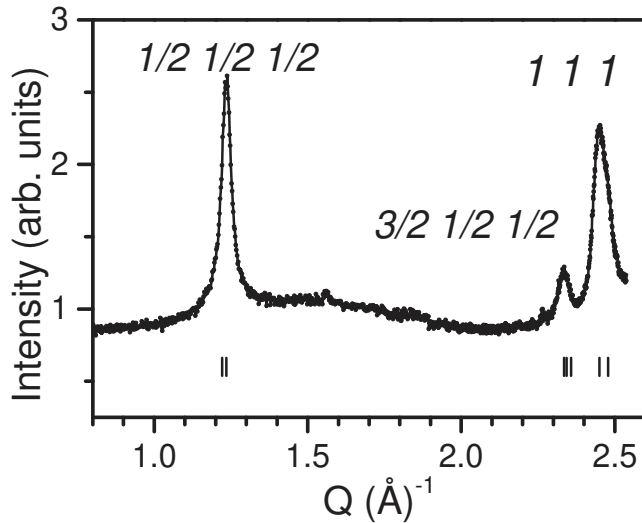


FIG. 1: Neutron diffraction patterns, observed (closed circles) and calculated (solid line) from MnO confined within SBA matrix with 47 Å channel diameter.

ensure that MnO predominantly occupies the channel voids. Neutron diffraction experiments were carried out at the diffractometer G6-1 of the Laboratoire Léon Brillouin at the Orphée reactor with a neutron wavelength of 4.732 Å.

B. Shape and dimension of magnetic domains

A typical neutron diffraction pattern measured at 10 K is shown in figure 1. To increase intensity we used a large neutron wavelength. However, in this case we could observe only two magnetic reflections: $\{\frac{1}{2} \frac{1}{2} \frac{1}{2}\}$ and $\{\frac{3}{2} \frac{1}{2} \frac{1}{2}\}$ and one nuclear reflection $\{111\}$.

With synchrotron and neutron diffraction it was shown that nuclear diffraction peaks from the samples with large channels (47-87 Å) are asymmetric and have a "saw-tooth" profile that is indicative of the two-dimensional shape of confined nanoparticle. It was shown that in this case, the confined nanoparticles have a shape of nanoribbons³.

However, the magnetic peaks appear to be symmetric for all samples. In order to evaluate the size of the magnetic domains from the peak broadening we used the Thompson-Cox-Hastings approximation of the line shape⁹ implemented into the program FULLPROF¹⁰. It is well known that the smaller dimensions of the nanoparticles contribute to the peak "pedestal", while the peak width is defined mainly by the larger dimensions. Therefore from the peak broadening we can evaluate only the length of the magnetic domains. Apparently the domain length in the case of large diameters (nanoribbons) should be underestimated because of an additional contribution to the peak broadening from a ribbon thickness. The lengths of magnetic domains are shown in figure 2.

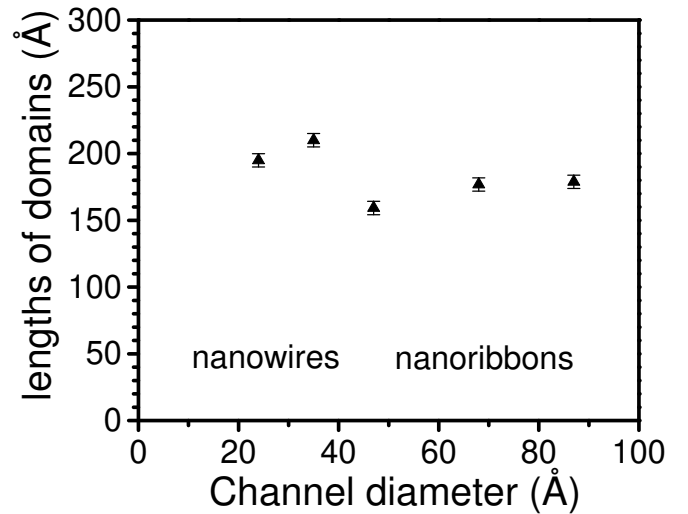


FIG. 2: The lengths of magnetic domains of MnO within the channels of different diameter.

Numerical calculations of the diffraction profiles, by the method used in ref.³, for the refined lengths of magnetic domains shows that in this case the expected peak asymmetry due to two-dimensional lattice⁸ is beyond experimental accuracy. However, the unit cell parameter refined from the positions of the magnetic reflections coincides with that of the bulk MnO, while the unit cell parameter refined from the position of the nuclear reflection appears noticeably smaller because of the Warren shift for a two-dimensional lattice³.

This means that in contrast with the nuclear particles the magnetic domains of smaller sizes should be considered as three-dimensional needle-shape objects.

Since the lengths of magnetic domains in the channels with different diameter appear to be practically the same, the main topological parameter responsible for anisotropy of the magnetic system should be the averaged magnetic domain diameter, which is slightly smaller than the channel diameter. This means that we are dealing with a system of magnetic objects with a variable dimensionality dependent on the channel diameter.

C. Magnetic moments and phase transitions

Fixing the scale factor refined in the paramagnetic region, the value of the ordered magnetic moments of confined MnO were calculated from the magnetic reflection intensity. These values are noticeably less than the free-ion value of $5\mu_B$ and the moment in the bulk $4.892 \mu_B/\text{ion}$ ¹¹. The magnetic moments for all samples appear to be similar in the limits of our statistical precision.

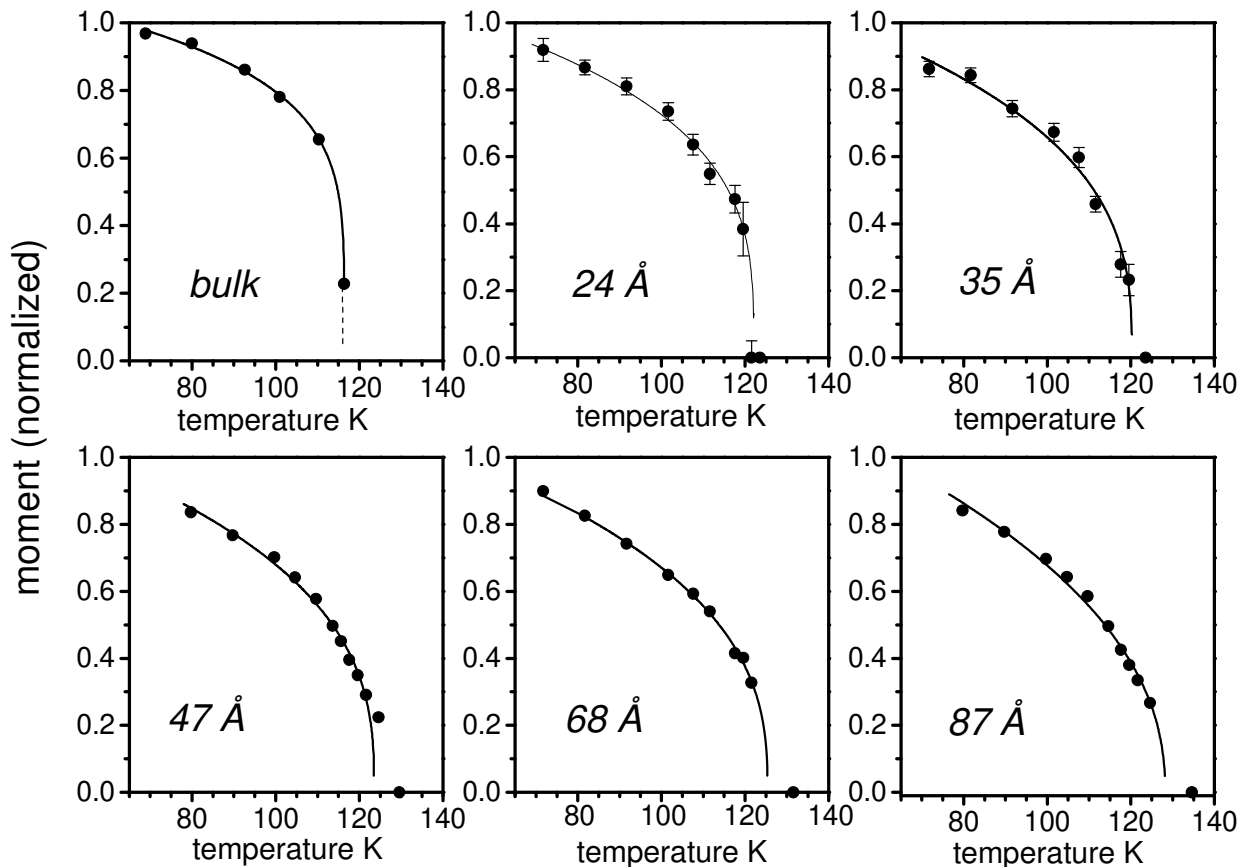


FIG. 3: Temperature dependence of the normalized magnetic moment for MnO confined to the channels of different diameter. Solid line corresponds to a fit with a power law. Errors (e.s.d.), if not shown, do not exceed the symbol size.

The mean value of $3.98(5) \mu_B/\text{ion}$ is close to $3.84(4) \mu_B/\text{ion}$ measured for MnO embedded in a porous glass¹. As well as in the latter case, the moment reduction can be explained by the disordering of the surface magnetic moments due to frustration effects.

The temperature dependencies of the magnetic moment measured for nanoparticles embedded in the matrices with different channel diameters are shown with the corresponding dependence for the bulk¹² in figure 3.

The nanoparticles embedded in the channels with diameters 45-97 Å are nanoribbons while nanoparticles within the channels with diameters 24-35 Å are nanowires. Nevertheless this topological difference does not appear in the results. The magnetic behavior is governed by the anisotropy of the shape, which, in turn, is defined by the ratio of the mean smallest dimension (proportional to the channel diameter) to the domain length.

In figure 3 it is seen that with decreasing channel diameter (and increasing anisotropy) the slope of the temperature dependence increases. The fitting of the magnetic moment with a power law $m \sim (T_N - T)^p$ demonstrates

that the exponent p and the temperature of transition T_N decrease with decreasing channel diameter (Figure 4a and 4b).

III. DISCUSSION

A. Reduction of dimensionality

The magnetic transition in MnO is accompanied by a rhombohedral crystal distortion, which lifts the frustration in the first coordination sphere and stabilizes the antiferromagnetic structure. This distortion provides the difference in the interactions between spins within the ferromagnetic layer and between antiferromagnetic spins in different ferromagnetic layers. It was shown by the random phase Green's function theory that this difference results in a first-order magnetic transition¹³.

From neutron profile refinements the values of structure distortion for all samples appear very similar, consequently a contraction mechanism cannot be responsible

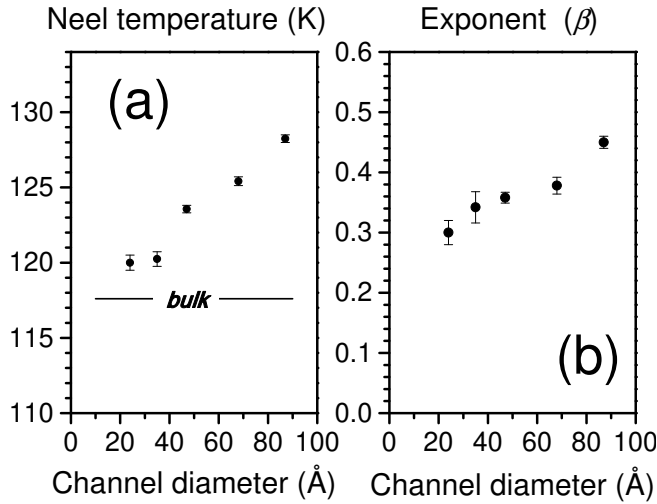


FIG. 4: Dependencies of Néel temperature (a) and exponent (b) on channel diameters from the fitting with a power law.

for the obvious transformation of the magnetic transition with channel diameter.

In figure 4b it is clear that firstly, the magnetic transition in confinement becomes continuous in contrast with the bulk. Secondly, it is clearly seen that there is a tendency to a reduction of the magnetic dimensionality. Because all magnetic domains differ only by the averaged diameter, the decreasing domain diameter could be responsible for the observed evolution of the continuous magnetic transition towards a discontinuous one due to reduction of dimensionality.

Obviously with an increasing channel diameter and nanoparticle diameter, the averaged magnetic correlation length should also increase. This explains the approach of the exponent value to the mean-field limit of 0.5¹⁴ in large channel diameters (Figure 4b).

In the studied matrices the nanochannels form a honeycomb lattice with a wall thickness between the adjacent channels about of only 8-10 Å. Therefore the magnetic interaction between nanoparticles in different channels should have an substantial impact on the magnetic behavior. It stabilizes critical fluctuations, which smooths the phase transition and can essentially enhance the effect of reduction of the dimensionality.

In MnO embedded within a porous glass¹ with large distance between the embedded nanoparticles (about 70-100 Å) there is no mutual interaction between nanoparticles which is consistent with the observed exponent value of 0.34(2) similar to the theoretical value of 0.326(4), obtained by the computer simulation of a finite-size scaling for 3D-Heisenberg models with nearest-neighbor interaction¹⁵.

The reduction of the transition temperature due to size effects is known in nanowires, and is attributed to the correlation length decreasing with a decrease in diameter¹⁶. Obviously the reduction of dimensionality with channel diameter also causes the decrease of the magnetic transi-

tion temperature. At $d \rightarrow 0$ the magnetic fluctuation destroys the long-range magnetic order and $T_N \rightarrow 0$. However, in our case we see that $T_N > T_{bulk}$ for all samples studied here which requires a more detailed analysis.

B. Ferromagnetic moment and its interaction with antiferromagnetic and structural order parameters

The magnetic phase transition in MnO is described by the 8-component order parameter corresponding to the 4-rays star of the wave vector $\mathbf{k} = [\frac{1}{2} \frac{1}{2} \frac{1}{2}] \cdot \frac{2\pi}{a}$, where a is a lattice constant. It was demonstrated by the renormalization-group technique that the Landau-Ginzburg-Wilson hamiltonian has no stable fixed points, that is consistent with a first-order phase transition observed in the bulk MnO¹⁷.

Another origin of the first-order phase transition could be a magnetostriction interaction, which should be taken into consideration due to experimentally observed softening of the elastic modulus c_{44} at the approach to the transition from above¹⁸. In this case the temperature region with developed critical fluctuations is not observed and one can expect the temperature dependence of sublattice magnetization corresponding to the mean-field approximation.

However, the experimentally observed values of exponents β (figure 4a) and the second-order transition (figure 3) give evidence that a fluctuation scenario dominates. Indeed, in nanoparticles one should expect the essential influence of the surface anisotropy on the phase transition due to the splitting of the multicomponent order parameter for a few order parameters of lower dimensionality, for which there is no theoretical restriction for the second order transition¹⁹.

A more difficult question is to determine which factors affect the temperature of magnetic transition, which in nanoparticles appears higher than those in the bulk (figure 4b) and increases with an increasing channel diameter.

Generally the boundary effects should decrease the transition temperature. Indeed, one should expect that in the vicinity of a free surface of crystallized nanoparticles of MnO, the absolute values of the exchange constants decrease due to frustration effects. In the phenomenology theory of a finite crystal this effect is described by the term of the positive surface energy in the thermodynamic potential^{20,21}. This term causes the decrease of the mean moment and the transition temperature at the surface that results in the decrease of the transition temperature of the entire nanoparticle.

However, on the other hand, because of the small dimensions of nanoparticle the translation symmetry is violated throughout the significant part of the nanoparticle volume. The crystal lattice of such objects can be considered as a set of condensed translation modes with the wave vectors in the interval $(1/a - 1/L)$, where L is the characteristic size of the nanoparticle. In this case

new interactions of the order parameter with other magnetic degrees of freedom, forbidden by the symmetry of the bulk, come into action. The similar situation, when structure distortions result in the appearance of a large number of sub-lattices within nanoparticle was modelled for NiO²².

Let us consider the phase antiferromagnetic transition in the ideal lattice corresponding to a high symmetric paramagnetic phase with "condensed" structural distortions, which are described by the order parameters η_{k_s} with the corresponding wave vectors \mathbf{k}_s ($s = 1, 2, \dots$). Generally the bilinear functions $\eta_{k_s} l_k$, where l_k are some antiferromagnetic critical order parameters, transforms according to a reducible representation $\Gamma(\mathbf{k}_s + \mathbf{k})$ of O_h group with the star of $\mathbf{k}_s + \mathbf{k}$.

Let us introduce a non-critical, secondary parameter $l'_{k'}$, forbidden by the symmetry of the undistorted lattice. It transforms accordingly to some irreducible representation $\Gamma'(\mathbf{k}')$ with $\mathbf{k}' = \mathbf{k}_s + \mathbf{k}$ contained in the reducible presentation $\Gamma(\mathbf{k}_s + \mathbf{k})$.

Because of symmetry the interaction between the structure distortion η_{k_s} , critical parameter l_k and non-critical parameter $l'_{k'}$, can be described by the bilinear invariant with respect to time inversion, namely, $\eta_{k_s} l_k l'_{k'}$.

As long as $\mathbf{k}_s + \mathbf{k} + \mathbf{k}' = 0$ in the case of $\mathbf{k}_s + \mathbf{k} = 0$ the secondary order parameters with $\mathbf{k} = 0$ will participate in the phase transition. This means that the antiferromagnetic phase transition will be accompanied by the appearance of the ferromagnetic moment M . Note that the net magnetic moment of individual nanoparticles could be provided as well by the uncompensated magnetic moments of different sub-lattices, as had been proposed by L. Néel²³.

Regardless of the origin of the net magnetic moment, its interaction with the antiferromagnetic order parameter can elevate the phase transition temperature which can be readily demonstrated in the framework of Landau theory.

Neglecting imperfections of nanoparticles in the first approximation we can consider the simplest thermodynamic potential:

$$\Phi = \Phi_0 + \frac{1}{2}\tau l_k^2 + \frac{1}{4}b l_k^4 + (f\eta_{k_s} l_k)M + \frac{1}{2}AM^2, \quad (1)$$

Here $b > 0$, $A > 0$ and f are some coefficients, $\tau = (T - T_{bulk})/T_{bulk}$. The free energy (1) can be minimized with respect to l_k and M . Since at the antiferromagnetic transition $\eta_{k_s} \rightarrow 0$ we obtain the following expression for the temperature of the antiferromagnetic transition:

$$T_N = T_{bulk} + \frac{(f\eta_{k_s})^2}{A}, \quad (2)$$

The interaction of the structural and magnetic order parameters can explain the increase in temperature of the antiferromagnetic transition.

There are some competitive factors which influence this temperature. Surface disordering of magnetic order leads a decrease of T_N , while the above mechanism of the ternary interactions leads to an increase of T_N . The experimentally observed increase in transition temperature with channel diameter shows that in the region of the studied matrices, the ternary interactions dominate. With an additional increase of channel diameter the temperature of the magnetic transition should decrease approaching the temperature of the bulk.

It should be emphasized that in the framework of Landau theory the ferromagnetic moment and the higher Néel temperature appear as being related. It is consistent with the observation of the small coercive fields in the same samples⁴. Moreover the ferromagnetic moment at the surface of the nanoparticles in spite of its antiferromagnetic core, should lead to super paramagnetic behavior of the ensemble of confined nanoparticles below the transition.

IV. CONCLUSION

Neutron diffraction studies of antiferromagnetic MnO confined within MCM-41 type channel matrices with channel diameters 24 - 87 Å show a magnetic behavior strongly different from that of the bulk. While a magnetic structure in confinement remains the same as in the bulk, the ordered magnetic moment is noticeably smaller and the magnetic phase transition is continuous with the increased Néel temperature T_N in contrast to the discontinuous first-order transition in the bulk.

With decreasing channel diameter the critical exponent in the temperature dependence of the magnetic moment linearly decreases. The confined nanoparticles have a needle-like shape of equal lengths. Therefore the observed transformation of the magnetic transition are attributed to the reduction of the magnetic dimensionality approaching the quasi one-dimensional case.

The transformation of the magnetic transition is accompanied by the decrease of T_N with the decrease in channel diameter. However, for all studied samples T_N remains higher than those for the bulk.

It is shown that the magnetic disordering and violation of the translation symmetry at the nanoparticle surface results in a ferromagnetic moment while the nanoparticle core remains antiferromagnetic. Taking into account the ternary interaction of this moment with the antiferromagnetic and associated structural order parameters the increased Néel temperature can be readily explained within in the framework of Landau theory.

Acknowledgments

The authors thank C. Alba-Simionesco, N. Brodie and G. Dosseh who prepared and characterized MCM and

SBA matrices. The work was supported by the RFBR (Grant 04-02-16550), the INTAS (Grant No. 2001-0826).

-
- ¹ I. V. Golosovsky, I. Mirebeau, G. André, D. A. Kurdyukov, Yu. A. Kumzerov, and S. B. Vakhrushev, *Phys. Rev. Lett.*, **86**, 5783 (2001)
 - ² M. E. Lines and E. D. Jones, *Phys. Rev.* **159**, 451 (1966).
 - ³ I. V. Golosovsky, I. Mirebeau, E. Elkaim, D. A. Kurdyukov and Y. A. Kumzerov, [arXiv:cond-mat/0503063](https://arxiv.org/abs/cond-mat/0503063).
 - ⁴ I. V. Golosovsky, D. Arčon, Z. Jagličič, P. Cevc, V. P. Sakhnenko, D. A. Kurdyukov and Y. A. Kumzerov, [arXiv:cond-mat/0503095](https://arxiv.org/abs/cond-mat/0503095).
 - ⁵ M. Grün, I. Lauer, and K. Unger, *Adv. Mater.*, **9**, 254 (1997).
 - ⁶ D. Zhao, J. Feng, Q. Huo, N. Melosh, G. H. Fredrickson, B.F. Chmelka, G. D. Stucky, *Science*, **279**, 548 (1998)
 - ⁷ D. Morineau, G. Dossen, C. Alba-Simionesco, *Phil. Mag. B*, **79**, 1845 (1999).
 - ⁸ B. E. Warren, *Phys. Rev.*, **59**, 693 (1941).
 - ⁹ P. Thompson, D. Cox, and B. Hastings, *J. Appl. Cryst.* **20**, 79 (1987).
 - ¹⁰ J. Rodriguez-Carvajal, *Physica B* **192**, 55, (1993). For a recent version of Fullprof, see: CPD Newsletters **26**, 12, (2001), available at <http://journals.iucr.org/iucr-top/comm/cpd/newsletters>
 - ¹¹ M. Bonfante, B. Hennion, F. Moussa and G. Pepy, *Solid State Commun.* **10**, 553, (1972).
 - ¹² C. G. Shull, W. A. Strauser and E. O. Wollan, *Phys. Rev.* **83**, 333, (1951).
 - ¹³ B. Morosin, *Phys. Rev. B* **1**, 236 (1970).
 - ¹⁴ H. Stanley, "Introduction to phase transitions and crytical phenomena", Clarendon Press, Oxford 1971.
 - ¹⁵ D. P. Landau, *J. Magn. Magn. Mater*, **200**, 231, (1999).
 - ¹⁶ L. Sun, P. C. Searson and C. L. Chien, *Phys. Rev. B* **61**, R6463 (2000).
 - ¹⁷ D. Mukamel, and S. Krinsky, *Phys. Rev. B* **13**, 5065, (1976).
 - ¹⁸ S. Miyahara, and D. Seino, *Physica B* **86-88**, 1128, (1977).
 - ¹⁹ E. Brézin, J. C. Le Guillou, and J. Zinn-Justin, *Phys. Rev. B* **10**, 892, (1974).
 - ²⁰ M. I. Kaganov, and A. N. Omelyanchouk, *Sov. Phys. JETP* **34**, 895, (1972).
 - ²¹ D. L. Mills, *Phys. Rev. B* **3**, 3887, (1971).
 - ²² R. H. Kodama, Salah A. Makhlof, and A. E. Berkowitz, *Phys. Rev. Lett.* **79**, 1393 (1997).
 - ²³ L. Néel, in *Low Temp. Phys.*, edited by C. Dewitt, B. Dreyfus, and P. D. de Gennes (Gordon and Breach, New York, 1962), p. 413.